

On the geometry of topological defects in glasses

Received: 23 April 2025

Accepted: 18 November 2025

Cite this article as: Wu, Z.W., Barrat, J.-L., Kob, W. On the geometry of topological defects in glasses. *Nat Commun* (2025). <https://doi.org/10.1038/s41467-025-66923-1>

Zhen Wei Wu, Jean-Louis Barrat & Walter Kob

We are providing an unedited version of this manuscript to give early access to its findings. Before final publication, the manuscript will undergo further editing. Please note there may be errors present which affect the content, and all legal disclaimers apply.

If this paper is publishing under a Transparent Peer Review model then Peer Review reports will publish with the final article.

On the geometry of topological defects in glasses

Zhen Wei Wu,¹ Jean-Louis Barrat,² and Walter Kob³

¹*Institute of Nonequilibrium Systems, School of Systems Science,
Beijing Normal University, 100875 Beijing, China*

²*Université Grenoble Alpes, CNRS, LIPhy, 38000 Grenoble, France*

³*Laboratoire Charles Coulomb, University of
Montpellier and CNRS, 34095 Montpellier, France*

(Dated: November 18, 2025)

Abstract

Recent studies have revealed a series of connections between the topological features of structural glasses and their material properties. These findings show a striking resemblance to results observed in quantum physics that underscore the significance of the nature of the wavefunction. However, so far the structural arrangement of the topological defects in glasses has remained elusive. Here, we investigate numerically the geometry and statistical properties of the topological defects related to the vibrational eigenmodes of a prototypical three-dimensional glass. We find that at low frequencies these defects form scale-invariant, quasi-linear structures and dictate the morphology of plastic events when the system is subjected to a quasi-static shear, i.e., the eigenmode geometry shapes the plastic behavior in 3D glasses. Our results indicate the presence of a profound connection between the topology of eigenmodes and plastic energy dissipation in disordered materials, thus generalizing the known link identified in crystalline materials.

email:

zwwu@bnu.edu.cn

jean-louis.barrat@univ-grenoble-alpes.fr

walter.kob@umontpellier.fr

INTRODUCTION

The vibrational and electronic energy spectra of materials have been in the focus of interest of many condensed matter physics studies since they are directly accessible in experiments, while the properties of the wave-functions, especially their phase, have received for long times much less attention [1–3]. However, recently things have changed dramatically, since it has been realized that these functions contain important information about the interference and superposition of quantum states, which allows to gain deep insight into the properties of condensed quantum materials [4–9]. Interestingly this shift of paradigm starts to occur also in the domain of glass physics. While in the past many studies focused on characterizing the vibrational density of states to rationalize the anomalous thermodynamic properties of glasses [10], only few investigations have looked into the nature of the eigenmodes. Most of these studies concentrated on the question whether or not these modes are localized or extended, a problem which is relevant for understanding the nature of the so-called boson-peak [11–17]. However, very recently it has been suggested that also the topological properties of a glass can give important insight into the thermodynamic and kinetic features of the material [18, 19]. One example is the demonstration that in two dimensions the geometry of the topological defects of the eigenvectors is closely correlated to the plastic response in amorphous matter [20], which has recently been verified experimentally in a 2D colloidal glass [21, 22]. Probing the topological properties of disordered materials is thus a promising approach to advance our understanding of these complex systems that have so far defied to reveal how their macroscopic behavior is connected to their microscopic structure [23].

It is important to realize that for a glass there is no unique way to define topological defects (TD) and so far it is not clear which definition is the most useful for gaining insight into a specific macroscopic property of the sample [20, 24–27]. Probing the influence of TDs on material properties is also hampered by the fact that some TD definitions are applicable only to two dimensional systems and cannot be generalized in a straightforward manner to $D = 3$. TDs arise, e.g., in the fields defined by the vibrational eigenvectors at the points in which the amplitude of the eigenfunction vanishes and hence its phase becomes undefined. Another example are TDs occurring in the displacement field generated when the sample is sheared, since then the trajectories of the particles can form loops around topological

vertices that can be transient or continuously reshaped by particle motion. For the cases of active matter and living systems its has, e.g., been well documented that topological defects in the displacement fields can influence the dynamics or pattern formation of the systems [28–32]. Note that these two types of TDs, i.e., in eigenvectors or displacement fields, differ not only in the nature of the field used to define them, but also by the fact that with the first definition one considers a mechanically stable configuration, while the second one deals with an out-of-equilibrium response. Understanding the relevance of these differences is therefore crucial for exploring topological quantities in the study of amorphous matter.

In this study, we numerically investigate for a prototypical three dimensional glass the geometry and statistical properties of eigenvectors associated with the vibrational eigenmodes, with a special focus on the TDs generated by these modes. Although the definition of these TDs is related to the one considered in an earlier study of 2D systems, we point out that the generalization to 3D is not a trivial step. We find that at low frequencies the spatial arrangement of these TDs form one-dimensional structures that have a scale-invariant geometry with a power-law exponent around $-5/3$, a value that can be rationalized from the quasi-linear structure of the filaments formed by the TDs, and hence is expected to be universal. When subjected to quasistatic shear, the resulting plastic events are strongly correlated with defects carrying a negative topological charge, revealing a close connection between TDs and plastic yielding. Remarkably, the spatial distribution of plastic events under shear mirrors the scaling behavior observed for the topological defects, reinforcing the idea that the eigenmode geometry plays a fundamental role for the plastic behavior of amorphous solids.

RESULTS

System

We study a binary mixture of Lennard-Jones particles, using a model that has been extensively investigated in the past [33], applying a small modification to avoid the crystallization at the lowest temperatures [34]. In the following we will use reduced units, reporting length and energy in terms of the size of the large particles and the well depth of the Lennard-Jones potential, respectively. The system, containing $N=800,000$ particles in a box of size

$(87.36)^3$, was equilibrated at a low temperature ($T = 0.43$), before it was cooled down to zero temperature. More details on the model and simulations are given in the Methods section.

Topological defects

The first 10,000 vibrational normal modes of the system are obtained by diagonalizing the Hessian matrix using ARPACK, see Methods for details. The lowest frequency is $\omega = 0.280$, while the highest one is 2.24, slightly below the main peak in the vibrational density of states, see Fig. 1 and Supplementary Fig. 1. To identify the topological defects of a given eigenvector with components (e_i^x, e_i^y, e_i^z) , $i = 1, \dots, N$, we first define a continuous vector field $\mathbf{u}(\mathbf{R})$ by interpolating between the positions of the particles:

$$\mathbf{u}(\mathbf{R}) = \sum_i w(\mathbf{R} - \mathbf{r}_i) \mathbf{e}_i / \sum_i w(\mathbf{R} - \mathbf{r}_i), \quad (1)$$

where \mathbf{r}_i is the location of particle i , \mathbf{e}_i is the eigenvector component for particle i , and w is a Gaussian weighting function, $w(\mathbf{R} - \mathbf{r}_i) = \exp(-|\mathbf{R} - \mathbf{r}_i|^2/\Delta^2)$, with a width of $\Delta = 1$. (The exact value of Δ is not crucial as long it is on the order of the size of a particle.) The topology of this vector field is then analyzed by projecting it on a cubic lattice of size $88 \times 88 \times 88$ superimposed to the sample (the length of the unit cell is thus ≈ 1). This lattice is subsequently used to identify the topological defects as follows, see Inset of Fig. 1: For each of the six square sides of a cubic unit cell, we search for a signature of a topological defect by examining the structure of the phase of the field $\mathbf{u}(\mathbf{R})$, after having it projected on the square, on the border of the plaquette via a line integral. If this integral gives a net change of $\pm 2\pi$ one has a vortex or an anti-vortex, while a charge zero corresponds to a field with no singularity. In practice we assign to each plaquette (having its corners at A, B, C , and D and being, e.g., in the xy -plane) a winding number $\nu_{x,y}$ defined as

$$\begin{array}{ccc} \theta_D & \longleftarrow & \theta_C \\ \downarrow & \nu_{x,y} & \uparrow \\ \theta_A & \longrightarrow & \theta_B \end{array} \quad \nu_{x,y} = [\Delta\theta_{A,B} + \Delta\theta_{B,C} + \Delta\theta_{C,D} + \Delta\theta_{D,A}] \mod 2\pi. \quad (2)$$

Here $\Delta\theta_{A,B}$ is the change of the phase θ from point A to B , and the angle θ_A at point A is given by angle formed by the vector (u_A^x, u_A^y) with the x -axis. Each plaquette contains either a vortex, an anti-vortex, or it is neutral, if $\nu_{x,y}$ is equal to 1, -1 , or 0, respectively. The search for topological defects is done for each of the six faces of the cubes of the lattice. For each box that is part of a vortex line, the vortex must enter from one face of the box and

exit from another face. Therefore, if the resolution of the discretization of the field $\mathbf{u}(\mathbf{R})$ is sufficiently high, there will be two faces, not necessarily opposite on the cube, that display a net phase change of 2π (or -2π), i.e., knowledge of whether two vortex points in neighboring planes form part of the same line is only limited by the spatial resolution. Ambiguities in the counting of the TD related to, e.g., nonzero winding on more than two faces of a voxel, can in principle be resolved by using a finer mesh. However, it turns out that with the mesh size we use the number of such cases is in practice very small and hence they do not alter the overall analysis in a significant manner. In the Supplementary Information (SI), this procedure is applied to simple synthetic vector fields, showing that it does indeed allow to identify vortex or antivortex lines. It is important to note that our detection procedure for the TDs is agnostic with regard to the geometrical arrangement of the defects, and in particular does not impose a line-like morphology for this arrangement. The procedure consists of two decoupled steps: We first locate zeros of the eigenvector field amplitude and assign a local topological index by evaluating the phase winding on each plaquette of the voxels. This step uses only local information and introduces no geometric bias. We then reconstruct connectivity by linking neighboring cells whose local indices are consistent. This reveals the intrinsic dimensionality of the zero set: Isolated zeros remain point-like; if zeros continue coherently across adjacent cells, a one-dimensional locus (TD line) emerges.

In Fig. 1 we show the number of topological defects per particle as a function of frequency ω . We observe that, at low ω , i.e., in the Debye-regime up to $\omega \approx 1.0$, one has the same ω^2 -dependence found in a 2D system [20]. This result indicates that as long as the system can be considered as an elastic continuum, the ω^2 -scaling between number of TDs and frequency is independent of the system dimension. To rationalize this ω^2 -dependence we show in Fig. 2 the TDs of the eigenmodes at different ω . For the lowest ω the eigenvectors are a superposition of transverse plane waves and this gives rise to TDs that align in (windy) one-dimensional structures, as can be recognized in the figure for $\omega = 0.28$. (Note that at finite ω the disorder of the system makes that these plane waves couple with each other, giving rise to the structures seen at low ω , see Supplementary Fig. 5 for a snapshot of the eigenvectors.) With increasing frequency the TD-lines become more and more complex and windy, but positive and negative lines are still clearly separated, indicating that they repel each other. At around $\omega = 0.567$ one sees the appearance of some clusters, i.e., positive and negative TD start to interfere with each other. Despite this interaction, the separation between positive

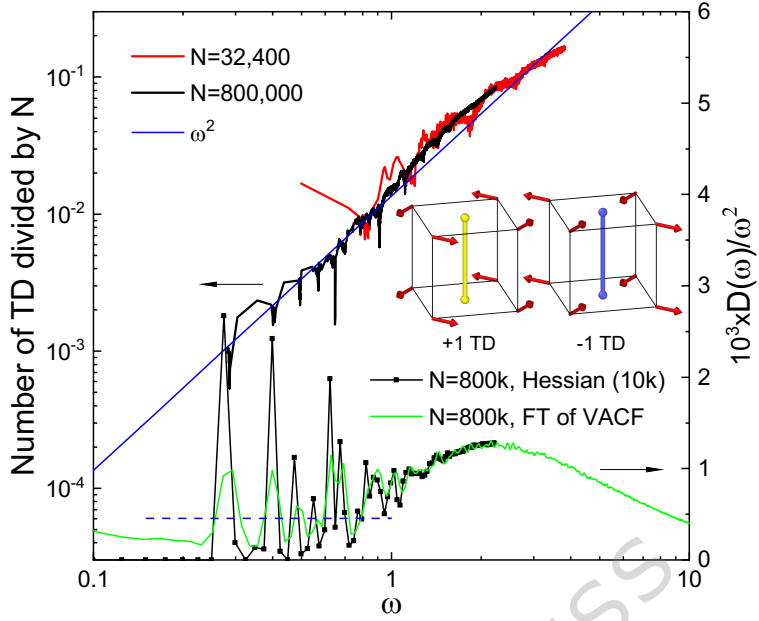


Fig. 1. Number of topological defects and vibrational density of states. Left scale: The number of TDs per particle as a function of frequency. For this we mesh the sample with a grid having a lattice size ≈ 1.0 and use it to identify the TDs. See main text and Inset for details. The red and black curve are the results from samples with $N = 800,000$ and $N = 32,400$, respectively, showing that finite size effects are not important. Right scale: Vibrational density of states $D(\omega)$ divided by ω^2 . $D(\omega)$ as obtained from the direct diagonalization of the Hessian matrix and from the time Fourier transform of the velocity auto-correlation function are shown as black line with symbols and green line, respectively. The horizontal blue dashed line denotes the Debye level calculated from the elastic properties of the sample (see Supplementary Table 1).

and negative TDs lines can be seen even at frequencies as high as $\omega = 1.21$, reflecting the local geometry of the acoustic modes. This regularity leads to a distance between lines of the order of the wavelength $\sim \omega^{-1}$, and to a scaling of the line density of ω^2 , rationalizing the ω^2 -dependence presented in Fig. 1, see also [20]. In general a superposition of plane waves can produce a variety of TD morphologies, depending on how the wave vectors are chosen [35]. In the low-frequency regime, the vibrational modes are predominantly transverse, and when the field is effectively a two-component (complex transverse) vector field, in three dimensions, the generic zero set of such a field has codimension 2 and thus forms line-like singularities. Consequently, the filamentary nature of TDs and the observed ω^2 -scaling emerge naturally from codimension and spectral arguments: the typical inter-line spacing scales as $\sim \omega^{-1}$,

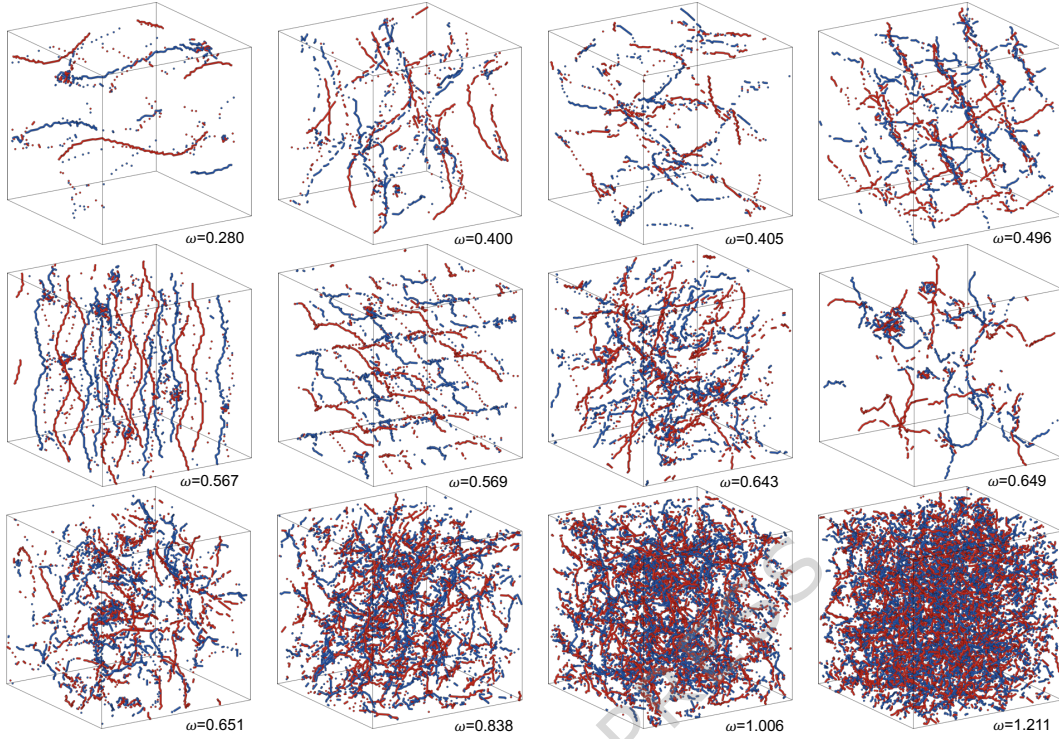


Fig. 2. Spatial arrangement of the topological defects. Topological filaments in a particular normal mode at different frequencies ω . Blue and red dots represent, respectively, TDs with winding number +1 and −1. Snapshots of the TD at higher frequencies are shown in Supplementary Fig. 6 of the SI, and Supplementary Fig. 6 also shows a zoom of the snapshot for $\omega = 1.211$. Most isolated dots in the panels are not genuine point singularities but cross-sections or short, sub-resolution pieces of vortex filaments introduced by the discrete grid. As one recognizes from the figure, these dots are not randomly dispersed but outline a one-dimensional structure; increasing spatial resolution (decreasing voxel size) causes them to approach each other thus outlining the one-dimensional structure better, see Supplementary Fig. 7 in the SI for a resolution-dependent illustration of this effect. Note that the filaments formed by the TDs do not end within the bulk of the sample arbitrarily, since for topological reasons this is forbidden. The apparent termination of these filaments is thus due to insufficient spatial resolution of the eigen-vector field or approaching line junctions.

yielding a line-length density $\sim \omega^2$. By contrast, isolated point singularities are rare events and do not influence significantly the scaling behavior. For the highest frequencies the TD no longer form long lines but complex patterns since their mutual interactions becomes very strong.

Spatial structure of the topological defects

To quantify the spatial arrangement of the TD lines we define a spatial correlation function of the topological defects of type $\alpha, \beta \in \{\pm 1\}$ at a given ω as,

$$g_{\alpha\beta}(r; \omega) = \frac{1}{N_\omega} \sum_{\kappa} g_{\kappa,\alpha\beta}(r) \delta(\omega - \omega_\kappa) . \quad (3)$$

Here $g_{\kappa,\alpha\beta}(r)$ is the pair correlation function characterizing the structure of TDs in the eigenmode κ , and N_ω is the number of modes in the system whose frequency lies in the range $\omega \pm \Delta\omega$, using $\Delta\omega = 0.086$. (This averaging is done in order to improve the statistics and the exact value of $\Delta\omega$ is not crucial.) Figure 3 demonstrates that, at fixed frequency, $g_{++}(r; \omega)$ and $g_{--}(r; \omega)$ are quite similar in that they display pronounced peaks at $r = 1$ and $\sqrt{2}$, positions that are independent of ω since they are given by the lattice, panels (a) and (b). These peaks become less pronounced with increasing frequency (Supplementary Fig. 8 shows these curves in a lin-lin plot) and the ω -dependence of the height of the main peak, $g_{\alpha\beta}^{\max}$, is presented in panel (d), demonstrating that for low ω the data for ++ and -- indeed track each other very well. Also notable is the fact that at small frequencies the height of the first peak is very large and seems to diverge for $\omega \rightarrow 0$, a consequence of the pronounced (quasi-linear) arrangement of the TDs. One intriguing feature of $g_{++}(r; \omega)$ and $g_{--}(r; \omega)$ is that the correlators exhibit within a significant range of r a scale-invariant behavior, i.e., a power-law, with an exponent around $-5/3$, independent of ω . Such a decay corresponds to a fractal dimension of $d_f = 4/3$ since the scaling of $g(r)$ for a fractal object of fractal dimension d_f is $g(r) \propto r^{d_f - d}$ [23]. Since the difference between $4/3$ and 1.0 is not large, the data of $g(r)$ indicates that in our 3D system, the TDs form quasi-one dimensional lines if ω is small, consistent with the snapshots of Fig. 2. (See Supplementary Fig. 9 for additional tests on the decay behavior of $g_{\alpha\beta}(r; \omega)$.) The exponent $d_f \approx 4/3$ reported here quantifies the line geometry of the TD set in 3D. In contrast, this arrangement has no direct analogue in 2D systems, in which topological defects are point-like. As argued in Ref. [20], in 2D the nature of the eigenvectors makes that the topological singularities are isolated points if the frequency is low. Thus these isolated zeros of the eigenvector field lack the extended connectivity required to form filamentary or self-affine structures. With increasing ω the range of scale-invariant behavior decreases, as indicated by the leveling-off of the correlation functions. The distance at which this leveling-off occurs defines a cross-over length ξ and

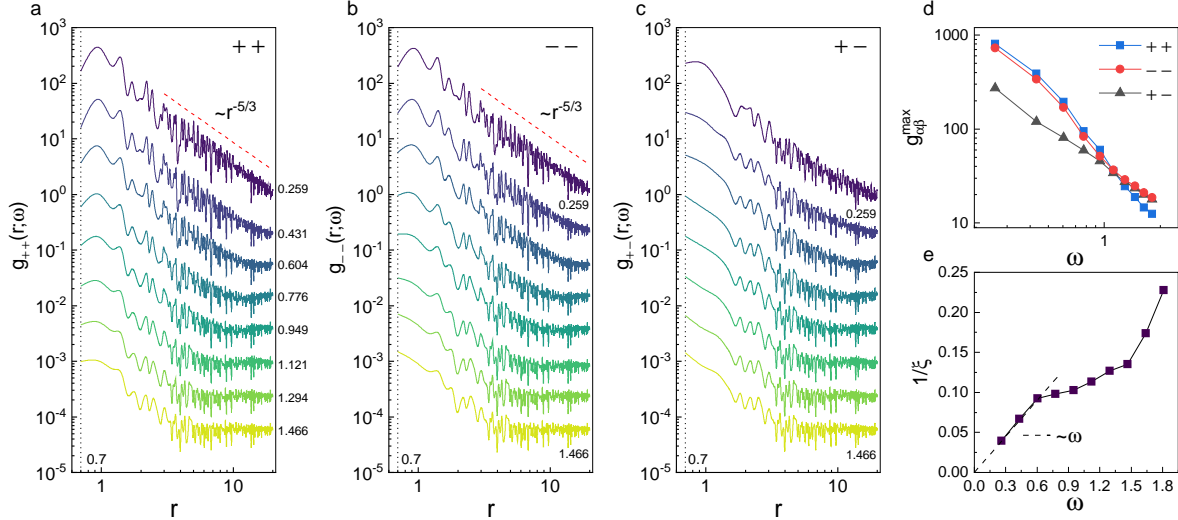


Fig. 3. Spatial correlations of the topological defects. **a-c:** Pair correlation functions for $++$, $--$, and $+-$ defect pairs at different values of ω , in which the frequency labels were given on the right-hand side of panel (a). Curves for $\omega > 0.259$ are shifted downward by multiple factors of 0.25 for visibility. The straight dashed line in panels (a) and (b) is a power-law with exponent $d_f - d = -5/3$, which gives for $d = 3$ a fractal dimension of $d_f = 4/3$. The vertical dotted line shows the correlation hole which is located at $r \approx \sqrt{2}/2$. **d** The ω -dependence of the height of the main peak in $g_{\alpha\beta}(r; \omega)$. **e** Inverse of the position of the level-off ξ in $g_{++}(r; \omega)$ as a function of frequency. The data at low-frequency display the expected linear behavior (dashed line) with a slope given by the average velocity-of-sound that can be calculated directly from the elastic moduli (Supplementary Table 1).

in Fig. 3e we present $1/\xi$ as a function of ω . One finds that for $\omega < 0.604$, this inverse length scale, which can be interpreted as a wave-vector characterizing the spacing of the TDs lines, is proportional to ω , in agreement with the presence of the acoustic modes with the ω^2 -scaling of the defects, as discussed above. We note that the slope of this linear part is given by the velocity of sound, supporting the view that at low ω this length scales is directly related to the acoustic modes. For intermediate frequencies one finds a much weaker dependence of ξ on ω , since in this ω -range one has a mixture between TDs lines that are well separated and zones in which the TDs strongly interact (see Fig. 2). For $\omega > 1.5$ the slope of the curve increases quickly, since the separation between the TD becomes very small.

The behavior of the function $g_{+-}(r; \omega)$ is different, panel (c). The correlation at $r = 1$ is about three times lower than the one of the TDs self-correlation, see panel (d), and also the amplitude of the oscillations at short distance is smaller, i.e., the short-range order is less pronounced. Interestingly the height of the correlator at small frequencies shows a weaker ω -dependence than the one found for the two other correlators. Furthermore Fig. 3d reveals a crossover behavior of $g_{--}^{\max}(\omega)$ at around $\omega=1.121$ in that for low frequencies the quantity tracks $g_{++}^{\max}(\omega)$ while at high frequency it follows the g_{+-}^{\max} curve. This cross-over frequency corresponds to the point in which the positive and negative TD start to interfere strongly, thus affecting the total number of TD at a given frequency.

Spatial structure of plastic events induced by shear

To probe the mechanical properties of the glass we have applied, at constant volume, an athermal quasi-static simple shear (using a strain increment of $\Delta\gamma = 0.0005$) and determined the stress-strain curve, Fig. 4a. We note that this curve shows no drops before reaching the very sharp yielding point at around strain $\gamma = 0.098$, indicating that the sample is large enough to avoid such finite size effects [36, 37]. Also included in the graph is the result if the strain increment is doubled, and one sees no qualitative difference. Supplementary Fig. 13 demonstrates that the sharp drop at global yielding gives rise to the formation of a very narrow shear band, which indicates that the system is rather brittle.

For a sheared configuration at strain γ , we calculate the non-affine displacement D_{\min}^2 [38] of the particles between two consecutive configurations that have a difference in strain of $\Delta\gamma = 0.0005$. For each particle i , we determine the largest non-affine displacement $\delta_i^{\max}(\gamma) = \max\{D_{\min}^2(i, \Delta\gamma), D_{\min}^2(i, 2\Delta\gamma), D_{\min}^2(i, 3\Delta\gamma), \dots, D_{\min}^2(i, \gamma)\}$ that was made by the particle up to the strain γ . We then select the particles having the top 0.5% of $\delta_i^{\max}(\gamma)$ and define them as plastic event (PE) particles at this γ . Figure 4b shows these PE particles for three different γ , sheared parallel to the xy -plane. At small γ , the PE particles are highly clustered, while with increasing strain, the distribution in space becomes more random. (Note that once the system has yielded, the PE particles are concentrated in a shear band.) In Fig. 4c we show the selected PE particles at strain $\gamma=0.01$ after shearing in three different directions and one recognizes that the three sets of particles are spatially highly correlated. This demonstrates that for the local yielding behavior the strain direction is not a relevant

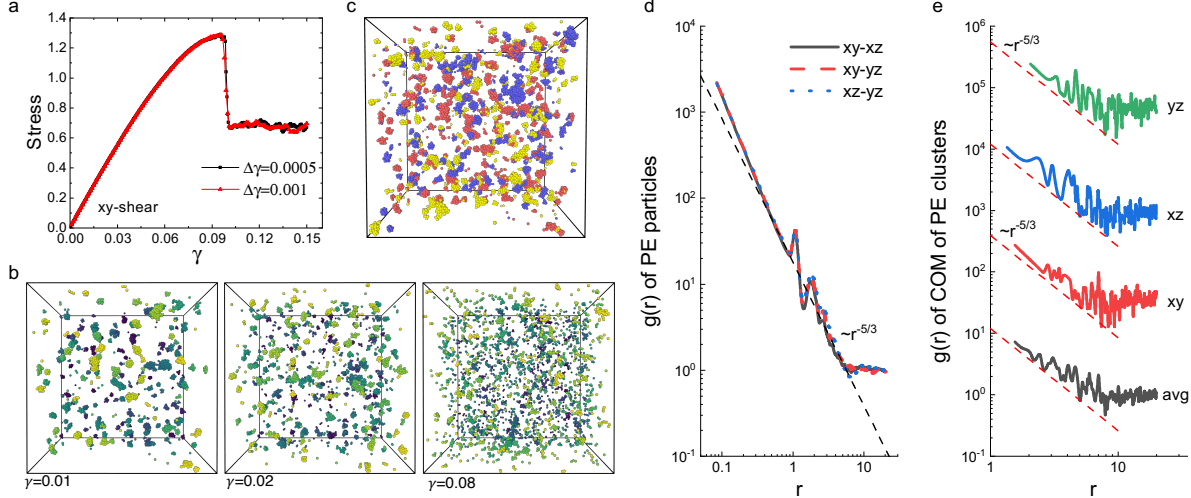


Fig. 4. Spatial arrangement of the plastic events. **a** The athermal quasi-static stress-strain curve obtained by using two different strain steps $\Delta\gamma$. **b** Configurations of PE particles at strain $\gamma=0.01$, 0.02 , and 0.08 after shearing the sample parallel to the xy -plane. The particles are color-coded to distinguish those in the foreground (bright) from those in the background (dark). **c** The configuration of PE particles at strain $\gamma=0.01$ after the sample has been sheared in the xy -, xz -, and yz -direction. The particles are colored in red, blue, and yellow, respectively, and one sees that the 3 type of PEs form tight clusters. **d** Spatial correlation between PE particles ($\gamma = 0.01$) generated by different shear direction. The dashed lines indicate a power-law with exponent $-5/3$. **e** Center of mass (COM) correlation of the PE clusters for different shear directions.

parameter, i.e., predicting the location of the PE can be done via a scalar quantity, an insight that is useful for developing theoretical approaches of yielding. This correlation can be quantified via the pair correlation function $g_{AB}(r)$ for the particles in the three sets, where $A, B \in \{x, y, z\}$ represents the set of PE particles generated under different shear directions, Fig. 4d. One recognizes that there is a strong spatial overlap between the PE particles in the three sets in that the peak height at small r exceeds $2 \cdot 10^3$, confirming the visual impression of panel (c). Interestingly one finds that this correlation function decays at intermediate distances with a power-law with an exponent that is compatible with $-5/3$, i.e., the value we found for the algebraic decay of the TD, see Fig. 3. This indicates that the PE particles and the TD are correlated to each other, and below we will see that this is indeed the case.

Further information on the spatial arrangement of the PE particles is obtained by de-

termining the center of mass of the clusters formed by these particles, and the resulting radial pair correlation function of these centers. For the cluster analysis we use a cutoff distance of 1.35, i.e., the location of the first minimum in the pair correlation function of the particles. Once more one finds, see Fig. 4e, that this correlation function shows a power-law decay and that the exponent is the same as the one obtained for the correlation between the TD. This remarkable agreement provides compelling evidence for a fundamental, previously unrecognized connection between microscopic eigenmode geometry and macroscopic plastic deformation. Thus, while the fact that the fractal dimension is close to 1.0 itself is not surprising, its coincidence with the fractal dimension characterizing the spatial patterns of plasticity substantially enhances our understanding of how eigenmode structures govern the mechanical behavior of amorphous solids. This correspondence, rather than the absolute value of d_f , is another important physical insight which indicates that the morphology of plastic rearrangements is organized by the pre-existing topology of low-frequency eigenmodes. This is thus strong evidence that the TDs and PE particles are closely related to each other and in the next section we will probe this connection in more detail.

Correlation between topological defects and plastic events

Previous studies have shown that TDs carrying negative topological charge are characterized by eigenvector flow fields corresponding locally to saddle-point configurations [20]. Physically, these configurations imply local mechanical instability: Under external perturbations such as shear, the delicate force balance at these points is readily disrupted, potentially triggering localized plastic rearrangements and hence one expects a noticeable correlation between such TDs and PE. The location of the PE particles can be correlated with the position of the topological defects of a given eigenmode κ by means of a corresponding radial distribution function $g_{\kappa,\alpha\text{PE}}(r)$, where $\alpha \in \{\pm 1\}$ denotes the nature of the TD ($g_{\kappa,\alpha\text{PE}}(r)$ is defined in Methods). In order to see how this spatial correlation function evolves with ω , we define an average correlation $g_{\alpha\text{PE}}(\omega; r)$ as

$$g_{\alpha\text{PE}}(r; \omega) = \frac{1}{N_\omega} \sum_{\kappa} g_{\kappa,\alpha\text{PE}}(r) \delta(\omega - \omega_{\kappa}) . \quad (4)$$

Here N_ω is the number of modes in the system whose frequencies are in the range $\omega \pm \Delta\omega$ using $\Delta\omega = 0.086$. (Also here the exact choice of $\Delta\omega$ is not crucial.) Figure 5a demonstrates that at low frequencies ($\omega \leq 0.43$) the PE particles and the positive TDs

are uncorrelated, while there is a noticeable short-range correlation with the negative TDs, results that are compatible with earlier findings in a two-dimensional systems [20] and reflect the $3D$ arrangement of the TD lines at low frequency discussed in Fig. 2. This correlation increases with ω and shows a broad maximum before peaking at around $\omega = 1.1$, i.e., there is a strong correlation between PEs and -1 TDs in the frequency interval of $0.604 < \omega < 1.294$, see Fig. 5b. Interestingly, this range coincides with the frequencies in which the TD lines start to fragment, i.e., where in Fig. 3e the ω -dependence of the length scale characterizing the size of the TD lines becomes less steep. We also note that at intermediate frequencies one observes a correlation between the PE particles and the positive TDs, the origin of which is the spatial correlation between the former and the -1 TDs, see Fig. 3c. For $\omega \approx 0.6$ the $g_{+PE}(r; \omega)$ has a peak at around $r \approx 0.7$, signaling that $+1$ and -1 TD pair together and create a dipole structure, a phenomenon also observed $2D$ [20]. In $3D$, these dipoles correspond to a local structure of TDs where two TDs with opposite topological charge occupy two different faces on the same unit cell of the coarse-graining grid.

The ω -dependence of g_{-PE}^{\max} suggests that the correlation between the TDs and the PE particles can be revealed best by averaging $g_{\alpha PE}(r)$ in the range $0.6 < \omega < 1.3$. For this we weight the modes with $1/\omega^2$, since this gives an equivalent weight to different frequencies. The resulting correlation functions $g_{+PE}^{av}(r)$ and $g_{-PE}^{av}(r)$ (see Methods for a definition) are shown in Fig. 5c and from this graph one clearly recognizes that at strain $\gamma=0.01$ the negative TDs are significantly correlated with the PE in that the peak at small r rises above 2.1, which means that there is a two-fold increase of the probability that a PE occurs close to a TD as compared to a uniform distribution. Also included in Fig. 5c is the γ -dependence of the correlation functions and one sees that at small γ the correlation is strong because the weakest spots in the sample are plastically deformed, and that upon approaching the yielding strain, $\gamma = 0.098$, the correlation is lost since the TD determined at $\gamma = 0$ are no longer a good predictor for the PEs.

In Fig. 5d we show the smoothed 3D topological charge density field $\Omega(\mathbf{R})$ (see Methods) at which the charge density is smaller than $-1.25 \cdot 10^{-4}$. The snapshot shows the intricate pattern the negative TDs form in space, indicating that the zones at which a plastic event occurs is highly complex. (Supplementary Fig. 11 shows the same type of graph for the TD field with high positive charge.) Figure 5e presents two representative slices from the corresponding topological charge density field, allowing to get a visual impression of the cor-

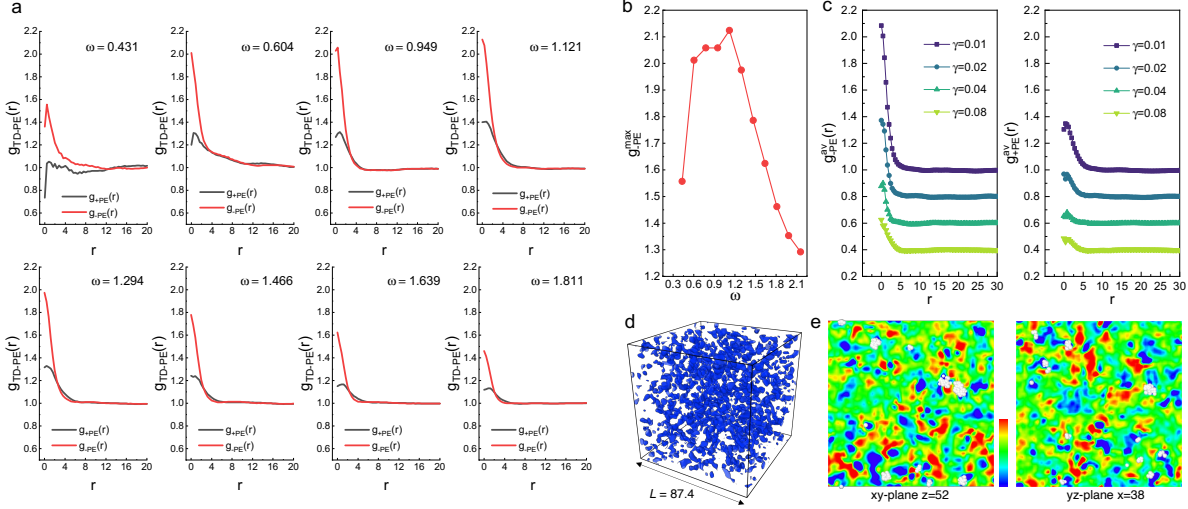


Fig. 5. Geometry of the eigenmodes shapes plasticity. **a** Spatial correlation functions between plastic events at strain $\gamma=0.01$ and topological defects with positive charge (black curve) and negative charge (red curve) for different frequencies. The PEs result from a shear in the xy -plane. **b** The maximum of $g_{-PE}(r; \omega)$ as a function of ω . **c** Weighted sums over ω of $g_{-PE}(r; \omega)$ and $g_{+PE}(r; \omega)$, left and right panel, respectively, for four different strains γ . The weights are ω^{-2} and all modes in the range $0.6 < \omega < 1.29$ have been taken into account. Curves are shifted downwards by multiples of 0.2 for the sake of visibility. **d** A 3D view of the isosurface of the smoothed charge density field $\Omega(\mathbf{R})$ with a iso-level value of $-1.25 \cdot 10^{-4}$. Note the presence of large holes in the structure which represent zones of little plastic activity. **e** Two slices to show the spatial correlation between PE (white spheres) and regions with larger negative TD charge density. The colorbar range is from $-1.25 \cdot 10^{-4}$ (blue) to $1.25 \cdot 10^{-4}$ (red).

relation between the location of the TDs and the PEs (marked as white spots superimposed to the maps). The graph demonstrates the strong correlation between zones with a high density of -1 TDs and the PEs. As already argued in Ref. [20], this correlation between -1 TDs and PEs is related to the fact that for such charges the local geometry of the normal mode field has a hyperbolic structure, see Supplementary Fig. 2 and 3, i.e., a small disturbance of the particle positions due to the shear will give rise in a significant change of the motion of the particle and hence most likely result in a PE.

DISCUSSION

In this work we have characterized the topology of vibrational eigenmodes in a three dimensional glass model. Our first important result is that the number of topological defects scales like ω^2 , which we relate to the fact that at low frequencies these defects are closely related to acoustic modes that form a surprisingly regular structure. Since well defined acoustic modes are present only in sufficiently large systems, this observation implies that the study of the geometrical arrangement of these topological defects, and hence the identification of the correlation between TDs and plastic events, should not be done in small systems since these do not include the acoustic-like modes that seem to be relevant for the mechanical properties of a macroscopic sample. Furthermore this insight suggests that in structural glasses plastic events cannot be understood solely as a local phenomenon with a response à la Eshelby, but should include correlation effects that are non-local, rationalizing the pronounced finite size effects found in the fracture of glasses [36]. Our results show that the soft spots at which the plastic events occur possess non-trivial spatial correlations, so that the PE cannot be regarded as local rearrangements that nucleate independently. The two-point correlator of PE positions exhibits a scale-free regime (Figs. 4d,e) with a power-law decay that mirrors the fractal organization of the TD network (Fig. 3), indicating that the soft spots are spatially organized by the pre-existing geometry of the eigenmodes rather than being just a random set. The fractal TD-line structure itself emerges from the interference of low-frequency acoustic modes, whose wavelength sets the inter-line spacing ($\sim \omega^{-1}$) and whose phase coherence gives rise to the long-range structure of the eigenvector field. It can be expected that, although the existence of a low-dimensional network of the PEs is due to the corresponding structure of the TDs, the PE structure becomes enhanced by the presence of elastic interactions that are long-ranged, inducing additional correlations in plastic activity along this geometry. Second, we have shown that the geometry of the topological defects displays scale-invariant behavior up to a frequency-dependent cutoff distance, with a fractal exponent close to 4/3, a feature that cannot be studied in 2D systems. While these features are obtained for the model glass investigated here, we expect that they reflect universal properties of the eigenmodes in elastic disordered systems since they are a direct consequence of the spatial structure of the acoustic modes. That the superposition of acoustic modes can give rise to a complex pattern of vortices in the displacement vector field,

has already been shown in Ref. [39], although in that study no connection with TDs was made. This observation supports thus the view that the results we have obtained regarding the structural arrangements of the TDs are generic.

Two recent studies have highlighted the use of TD in amorphous systems. Bera *et al.* [26] identified isolated point defects using the non-affine displacement field in 2D slices of a 3D sample, and observed a temporal correlation with plastic flow. Subsequently this group introduced a 3D hedgehog defect [27], and found that at low frequencies the number of such defects increases like ω^2 and that the location of these defects in non-affine displacements correlates well with plastic events of the sheared system, in qualitative agreement with our findings. However, instead of focusing on isolated point defects, we reconstruct their connectivity into extended, quasi-linear TD lines that capture the spatial continuity and network geometry of TDs, features that are inaccessible to slice-based or point-wise analyses. Our insight into the spatial arrangement of the TD allows us to reveal that these TD networks are scale-invariant at low frequencies, with an inter-line spacing scaling as $\sim \omega^{-1}$ and line density $\sim \omega^2$, consistent with acoustic wave interference in disordered media.

Using the identification of topological defects related to the vibrational modes, and inspired by previous studies in 2D [20], we have studied the correlation between the TDs and the plastic events that occur under shear deformation. A strong correlation between negative defects and plastic events is found, as in the case of 2D, and the spatial distribution of the PEs shows the same power-law as the TDs, which indicates that plasticity is encoded in the vibrational structure. Such a connection between quasi-linear topological defects and plasticity is reminiscent of the case of plasticity in crystals. Dislocations in crystals, acting as primary carriers of plastic deformation, result from distortions in the underlying order parameter, i.e., crystalline symmetry, characterized by Burgers vectors and slip planes [40]. In contrast, the TDs related to the eigenmodes of glasses do not form a regular lattice and arise from the superposition of acoustic waves (interacting with local disorder) rather than from a broken translational symmetry. This irregularity of the spatial arrangement of the TDs implies that their dynamics (when the sample is a bit perturbed) and interactions is more complex and less predictable than in crystalline systems. In the context of yielding of glassy materials, in recent experiments where the samples were subjected to pure shear, the TDs did form filamentary structures before condensating into shear bands [22]. These results hint that it is indeed possible to probe in real systems the spatial arrangement of the

TDs and therefore to test whether they do indeed show the fractal structure that we predict from our study.

Note that in the present work we have only probed the correlation between the location of the TDs and those of the PEs. In principle it is possible to take also into account the strength of the topological singularity and this might permit to improve the mentioned correlation. Such an analysis is, however, beyond the scope of the present work and is thus left to future investigations. It is also important to clarify that we do not claim that the identified correlation between the location of TD and PE make the TDs the best predictor regarding the occurrence of PEs. The quality of such a prediction would have to be assessed by following the approach by Richard *et al* [41], work that is outside the scope of the present study. Our result do instead establish a valuable connection between well-defined physics based quantities, the TDs, and mechanical response of the system.

In recent years, various machine learning (ML) approaches, both supervised and unsupervised, have been employed to detect and quantify structural heterogeneities and defect-like regions in glass-forming systems [42–46]. While these methods have yielded valuable insights into dynamic heterogeneity and plasticity, they often require a large number of microscopic descriptors. In contrast, our approach leverages quantities derived from vibrational eigenmodes to identify topological defects without supervision or descriptors, allowing for a more transparent, physically interpretable characterization. This simplicity of our method facilitates to establish a clearer connection between microscopic eigenmode geometry and emergent plasticity morphology. In this way, our results not only extends the insights gained from ML-based frameworks but may also offer useful insights for constructing more interpretable [47, 48], physics-informed ML models for amorphous materials.

In the future it will be important to investigate how the arrangement of the TDs is related to the brittleness of the glass since this might allow to make prediction of this important material properties directly from the unsheared sample. In addition it can be expected that also the nature of the fracture occurring beyond the yielding point is related to the presence of the TDs, with zones that have a high local density of positive TDs being avoided by the fracture front since they are mechanically more stable. Also the evolution of the geometrical arrangement of the TDs under cyclic shear is an important question, since it should allow to gain important insight into the aging behavior of glasses under mechanical stress.

We also point out that recent research on the generation of ultra-stable glasses [49],

utilizing techniques such as random pinning/bonding [50–53], highlights the important role of quenched disorder in the vitrification process, see also Ref. [54, 55]. It is thus tempting to speculate that the topological defects with positive charge can be considered to be a kind of quenched disorder that is related to the slowing down of the dynamics of the glass-former since these defects are in regions that are mechanically stable. Hence it will also be of interest to characterize the details of the geometry of the structure formed by the TDs, such as length of TD segments, angles between such segments, local densities, etc. This idea merits further exploration, as it offers a potentially interesting novel approach to predict the phenomenon of dynamic heterogeneity—one of the hallmark behaviors observed in supercooled liquids approaching the glass transition, as well as the dynamic slowing-down.

The linear arrangement of TDs that we have documented here can be found also in other fields of physics such as the vortex lines representing topological singularities in quantum fluids/gases, where interference and phase factor of varying waves play an important role. These features are robust and at the origin of energy cascades and dissipation processes that exhibits a scale-invariant behavior [56, 57], making them a fundamental ingredient in wave-based systems. The scale-invariance that we have identified in the spatial organization of our TDs hints therefore at a possible universality regarding how defects organize and interact across a wide range of physical systems. Scale invariance is a hallmark of critical phenomena, and its presence in amorphous materials suggests that plasticity and deformation processes might be related to critical-like/avalanche behavior [58–61] in which the system exhibits self-similar organization across different length scales. This might imply that the plastic behavior (or energy dissipation) of materials, whether crystalline [62], amorphous, or polycrystalline, follows universal scaling laws that are independent of the specific material but instead depend only on the topology and elastic properties of the system.

METHODS

MD Simulation. The simulations were carried out for a system with $N=800,000$ and we used a potential that is a slight modification of the standard Kob-Andersen potential. This modification (an addition of a linear term to the original potential) was proposed by Schröder and Dyre and has the effect that crystallization is (so far) completely avoided [34].

We equilibrated the system at $T = 0.430$ ($T_{\text{MCT}}=0.436$) for 30 million steps (density was 1.200 and step size was 0.005) and then cooled the sample to $T = 0$ within 30 million time steps. This slow cooling schedule ensures that the resulting samples are well-annealed and representative of stable glasses, as supported by previous studies [36] and confirmed by our stress-strain response (Supplementary Fig. 11) which exhibits sharp yielding transitions characteristic of well-annealed, mechanically stable glasses [63]. These features indicate the robustness and reproducibility of the mechanical and topological analyses reported in this work.

Normal Modes. A conjugate gradient energy minimization process was used to get the inherent structure of the configuration, and subsequently the vibrational normal modes were obtained by diagonalizing the dynamical matrix \mathcal{D} which is defined as

$$\mathcal{D} = \frac{1}{\sqrt{m_i m_j}} \frac{\partial^2 U(\mathbf{r}^N)}{\partial \mathbf{r}_i \partial \mathbf{r}_j}. \quad (5)$$

Here $U(\mathbf{r}^N)$ is the total potential energy of the system and m_i is the mass of particle i , and all masses were set to 1.0. We calculated the first (lowest frequency) 10^4 eigenmodes for the system with $N = 800,000$ with ARPACK. The vibrational density of states $D(\omega)$ were calculated as

$$D(\omega) = (1/3N) \sum_{\kappa} \delta(\omega - \omega_{\kappa}). \quad (6)$$

Correlation function between the TDs and the PEs. For each eigenmode $\kappa = 1, 2, \dots, 3N$, we define the radial pair correlation function $g_{\kappa,\alpha\text{PE}}(r)$ between the TDs and PEs, with $\alpha \in \{-1, +1\}$, as

$$g_{\kappa,\alpha\text{PE}}(r) = \frac{L^3}{4\pi r^2 N_{\text{TD}} N_{\text{PE}}} \sum_{i=1}^{N_{\text{TD}}} \sum_{j=1}^{N_{\text{PE}}} \delta(r - |\mathbf{r}_{ij}|). \quad (7)$$

Here N_{TD} and N_{PE} are the number of TDs of the mode κ and the number of particles associated to PEs, respectively, and r_{ij} is the distance between the TD i and the PE j . Since the number of TDs increases quadratically with ω , the average correlation function $g_{\alpha\text{PE}}^{\text{av}}(r)$ is then defined by

$$g_{\alpha\text{PE}}^{\text{av}}(r) = \frac{\sum_{\kappa} g_{\kappa,\alpha\text{PE}}(r)/\omega_{\kappa}^2}{\sum_{\kappa} 1/\omega_{\kappa}^2}, \quad (8)$$

where the sum over κ runs over the ω -range defined in the main text.

Generating of 3D topological charge density field. To get more insight into the geometry of the eigenmodes, it is useful to introduce a density field that is a weighted average over the topological charges in the system. Since the TD are defined via the plaquettes given in Eq. (2), i.e., they have orientational information on the eigenvector field, we keep track of this information by taking the average only in the plane of the plaquette. The weighted density field of the TDs at position \mathbf{R} is thus given by $\Omega(\mathbf{R}) = \Omega_{xy}(\mathbf{R}) + \Omega_{xz}(\mathbf{R}) + \Omega_{yz}(\mathbf{R})$, where, e.g., the field Ω_{xy} is defined by

$$\Omega_{xy}(\mathbf{R}) = \frac{1}{N} \sum_{\kappa} \frac{1}{\omega_{\kappa}^2} \sum_{i(\kappa)} \frac{\nu_{i,xy}}{|\mathbf{r}_i - \mathbf{R}|} \Pi(z_i - Z) . \quad (9)$$

(The fields Ω_{xz} and Ω_{yz} are defined analogously.) Here $\mathbf{R} = (X, Y, Z)$, N is the number of particles contained in the system, ω_{κ} is the frequency of mode κ and $\nu_{i,xy}$ is the topological charge (+1 or -1) of the i -th TD, located at the point (x_i, y_i, z_i) , in the xy -plane of mode κ . The function $\Pi(z_i - Z)$ is a rectangle function (with a width of the discretization of the field) which assures that the TDs are only visible in the xy -plane, but not outside of this plane. Thus essentially each TD is multiplied with a planar $1/r$ -type convolution kernel function which smooths it spatially over some length scales in the plane it belongs to. This smoothening process quantifies the influence of a topological charge ν placed at a distance r , which in our case has the physical meaning of measuring how much the local orientation of the field varies on a circular circuit of radius r around the defect core, hence taking into account the interference effect between different TDs. In practice, we set the range of action of the $1/r$ -kernel as $1 < |r| < L/2$, where L is the size of the simulation box.

Data Availability

The datasets generated during and/or analysed during the current study are available from the corresponding author on request. See also here: <https://zenodo.org/records/17628809>.

- [1] Fock, V. Über die Beziehung zwischen den Integralen der quantenmechanischen Bewegungsgleichungen und der Schrödingerschen Wellengleichung. *Zeitschrift für Physik* **49**, 323–338 (1928).
- [2] Bohm, A., Mostafazadeh, A., Koizumi, H., Niu, Q. & Zwanziger, J. *The Geometric Phase in*

Quantum Systems – Foundations, Mathematical Concepts, and Applications in Molecular and Condensed Matter Physics (Springer Science & Business Media, 2013).

- [3] Törmä, P. Essay: Where can quantum geometry lead us? *Phys. Rev. Lett.* **131**, 240001 (2023).
- [4] Thouless, D. J., Kohmoto, M., Nightingale, M. P. & den Nijs, M. Quantized Hall conductance in a two-dimensional periodic potential. *Phys. Rev. Lett.* **49**, 405–408 (1982).
- [5] Haldane, F. D. M. Nobel lecture: Topological quantum matter. *Rev. Mod. Phys.* **89**, 040502 (2017).
- [6] Hasan, M. Z. & Kane, C. L. Colloquium: Topological insulators. *Rev. Mod. Phys.* **82**, 3045–3067 (2010).
- [7] Qi, X.-L. & Zhang, S.-C. Topological insulators and superconductors. *Rev. Mod. Phys.* **83**, 1057–1110 (2011).
- [8] Zhang, L. & Niu, Q. Chiral phonons at high-symmetry points in monolayer hexagonal lattices. *Phys. Rev. Lett.* **115**, 115502 (2015).
- [9] Zhang, T. *et al.* Double-weyl phonons in transition-metal monosilicides. *Phys. Rev. Lett.* **120**, 016401 (2018).
- [10] Ramos, M. A. *Low-Temperature Thermal and Vibrational Properties of Disordered Solids* (World Scientific, 2022).
- [11] Schober, H., Oligschleger, C. & Laird, B. Low-frequency vibrations and relaxations in glasses. *J. Non-Cryst. Solids* **156**, 965–968 (1993).
- [12] Schober, H. R. & Oligschleger, C. Low-frequency vibrations in a model glass. *Phys. Rev. B* **53**, 11469–11480 (1996).
- [13] Mazzacurati, V., Ruocco, G. & Sampoli, M. Low-frequency atomic motion in a model glass. *Europhys. Lett.* **34**, 681–686 (1996).
- [14] Schober, H. R. & Ruocco, G. Size effects and quasilocalized vibrations. *Philos. Mag.* **84**, 1361–1372 (2004).
- [15] Xu, N., Vitelli, V., Liu, A. J. & Nagel, S. R. Anharmonic and quasi-localized vibrations in jammed solids—modes for mechanical failure. *Europhys. Lett.* **90**, 56001 (2010).
- [16] Chen, K. *et al.* Measurement of correlations between low-frequency vibrational modes and particle rearrangements in quasi-two-dimensional colloidal glasses. *Phys. Rev. Lett.* **107**, 108301 (2011).

- [17] Tong, H. & Xu, N. Order parameter for structural heterogeneity in disordered solids. *Phys. Rev. E* **90**, 010401 (2014).
- [18] Nussinov, Z., Weingartner, N. & Nogueira, F. The “glass transition” as a topological defect driven transition in a distribution of crystals and a prediction of a universal viscosity collapse. In *Topological Phase Transitions and New Developments*, 61–79 (World Scientific, 2019).
- [19] Vasin, M. G. Glass transition as a topological phase transition. *Phys. Rev. E* **106**, 044124 (2022).
- [20] Wu, Z. W., Chen, Y., Wang, W.-H., Kob, W. & Xu, L. Topology of vibrational modes predicts plastic events in glasses. *Nat. Commun.* **14**, 2955 (2023).
- [21] Vaibhav, V. *et al.* Experimental identification of topological defects in 2d colloidal glass. *Nat. Commun.* **16**, 55 (2025).
- [22] Wang, X., Shang, J., Wang, Y., Zhang, J. & Baggioli, M. Topological defects govern plasticity and shear band formation in two-dimensional amorphous solids. *arXiv preprint arXiv:2507.03771* (2025).
- [23] Binder, K. & Kob, W. *Glassy Materials and Disordered Solids: Introduction to Their Statistical Mechanics* (World Scientific, Singapore, 2011).
- [24] Baggio, M., Kriuchevskyi, I., Sirk, T. W. & Zacccone, A. Plasticity in amorphous solids is mediated by topological defects in the displacement field. *Phys. Rev. Lett.* **127**, 015501 (2021).
- [25] Desmarchelier, P., Fajardo, S. & Falk, M. L. Topological characterization of rearrangements in amorphous solids. *Phys. Rev. E* **109**, L053002 (2024).
- [26] Bera, A. *et al.* Clustering of negative topological charges precedes plastic failure in 3d glasses. *PNAS nexus* **3**, pgae315 (2024).
- [27] Bera, A., Zacccone, A. & Baggio, M. Hedgehog topological defects in 3d amorphous solids. *Nat. Commun.* **16**, 5990 (2025).
- [28] Peng, C., Turiv, T., Guo, Y., Wei, Q.-H. & Lavrentovich, O. D. Command of active matter by topological defects and patterns. *Science* **354**, 882–885 (2016).
- [29] Saw, T. B. *et al.* Topological defects in epithelia govern cell death and extrusion. *Nature* **544**, 212–216 (2017).
- [30] Beliaev, M., Zöllner, D., Pacureanu, A., Zaslansky, P. & Zlotnikov, I. Dynamics of topological defects and structural synchronization in a forming periodic tissue. *Nat. Phys.* **17**, 410–415 (2021).

- [31] Maroudas-Sacks, Y. *et al.* Topological defects in the nematic order of actin fibres as organization centres of hydra morphogenesis. *Nat. Phys.* **17**, 251–259 (2021).
- [32] Copenhagen, K., Alert, R., Wingreen, N. S. & Shaevitz, J. W. Topological defects promote layer formation in myxococcus xanthus colonies. *Nat. Phys.* **17**, 211–215 (2021).
- [33] Kob, W. & Andersen, H. C. Testing mode-coupling theory for a supercooled binary Lennard-Jones mixture I: The van Hove correlation function. *Phys. Rev. E* **51**, 4626–4641 (1995).
- [34] Schröder, T. B. & Dyre, J. C. Solid-like mean-square displacement in glass-forming liquids. *J. Chem. Phys.* **152**, 141101 (2020).
- [35] O'holleran, K., Padgett, M. J. & Dennis, M. R. Topology of optical vortex lines formed by the interference of three, four, and five plane waves. *Optics Express* **14**, 3039–3044 (2006).
- [36] Zhang, Z., Ispas, S. & Kob, W. The critical role of the interaction potential and simulation protocol for the structural and mechanical properties of sodosilicate glasses. *J. Non-Cryst. Solids* **532**, 119895 (2020).
- [37] Richard, D., Rainone, C. & Lerner, E. Finite-size study of the athermal quasistatic yielding transition in structural glasses. *J. Chem. Phys.* **155**, 056101 (2021).
- [38] Falk, M. L. & Langer, J. S. Dynamics of viscoplastic deformation in amorphous solids. *Phys. Rev. E* **57**, 7192–7205 (1998).
- [39] Lerner, E. & Bouchbinder, E. Testing the heterogeneous-elasticity theory for low-energy excitations in structural glasses. *Phys. Rev. E* **111**, L013402 (2025).
- [40] Taylor, G. I. The mechanism of plastic deformation of crystals. Part i.—theoretical. *Proc. R. soc. Lond. Ser. A, Contain. Pap. Math. Phys. Character.* **145**, 362–387 (1934).
- [41] Richard, D. *et al.* Predicting plasticity in disordered solids from structural indicators. *Phys. Rev. Mater.* **4**, 113609 (2020).
- [42] Cubuk, E. D. *et al.* Identifying structural flow defects in disordered solids using machine-learning methods. *Phys. Rev. Lett.* **114**, 108001 (2015).
- [43] Schoenholz, S. S., Cubuk, E. D., Sussman, D. M., Kaxiras, E. & Liu, A. J. A structural approach to relaxation in glassy liquids. *Nat. Phys.* **12**, 469–471 (2016).
- [44] Bapst, V. *et al.* Unveiling the predictive power of static structure in glassy systems. *Nat. Phys.* **16**, 448–454 (2020).
- [45] Ronhovde, P. *et al.* Detecting hidden spatial and spatio-temporal structures in glasses and complex physical systems by multiresolution network clustering. *Eur. Phys. J. E* **34**, 105

- (2011).
- [46] Ronhovde, P. *et al.* Detection of hidden structures for arbitrary scales in complex physical systems. *Sci. Rep.* **2**, 329 (2012).
 - [47] Boattini, E. *et al.* Autonomously revealing hidden local structures in supercooled liquids. *Nat. Commun.* **11**, 5479 (2020).
 - [48] Boattini, E., Smallenburg, F. & Filion, L. Averaging local structure to predict the dynamic propensity in supercooled liquids. *Phys. Rev. Lett.* **127**, 088007 (2021).
 - [49] Ediger, M. D. Perspective: Highly stable vapor-deposited glasses. *J. Chem. Phys.* **147** (2017).
 - [50] Kob, W. & Berthier, L. Probing a liquid to glass transition in equilibrium. *Phys. Rev. Lett.* **110**, 245702 (2013).
 - [51] Ozawa, M., Kob, W., Ikeda, A. & Miyazaki, K. Equilibrium phase diagram of a randomly pinned glass-former. *Proc. Natl. Acad. Sci.* **112**, 6914–6919 (2015).
 - [52] Ozawa, M., Iwashita, Y., Kob, W. & Zamponi, F. Creating bulk ultrastable glasses by random particle bonding. *Nat. Commun.* **14**, 113 (2023).
 - [53] Ozawa, M., Barrat, J.-L., Kob, W. & Zamponi, F. Creating equilibrium glassy states via random particle bonding. *J. Stat. Mech.* **2024**, 013303 (2024).
 - [54] Dyre, J. C. Solid-that-flows picture of glass-forming liquids. *J. Phys. Chem. Lett.* **15**, 1603–1617 (2024).
 - [55] Lubomirsky, Y. & Bouchbinder, E. Quenched disorder and instability control dynamic fracture in three dimensions. *Nat. Commun.* **15**, 7494 (2024).
 - [56] Barenghi, C. F. Tangled vortex lines: dynamics, geometry and topology of quantum turbulence. In *Knotted Fields*, vol. 2344, 243–279 (Springer, 2024).
 - [57] Kolmogorov, A. N. A refinement of previous hypotheses concerning the local structure of turbulence in a viscous incompressible fluid at high reynolds number. *J. Fluid Mech.* **13**, 82–85 (1962).
 - [58] Nicolas, A., Ferrero, E. E., Martens, K. & Barrat, J.-L. Deformation and flow of amorphous solids: Insights from elastoplastic models. *Rev. Mod. Phys.* **90**, 045006 (2018).
 - [59] Budrikis, Z., Castellanos, D. F., Sandfeld, S., Zaiser, M. & Zapperi, S. Universal features of amorphous plasticity. *Nat. Commun.* **8**, 15928 (2017).
 - [60] Lehtinen, A., Costantini, G., Alava, M. J., Zapperi, S. & Laurson, L. Glassy features of crystal plasticity. *Phys. Rev. B* **94**, 064101 (2016).

- [61] Sun, B. A. *et al.* Plasticity of ductile metallic glasses: a self-organized critical state. *Phys. Rev. Lett.* **105**, 035501 (2010).
- [62] Huang, L.-Z., Wang, Y.-J., Jiang, M.-Q. & Baggiooli, M. Spotting structural defects in crystals from the topology of vibrational modes. *J. Mech. Phys. Solids* **204**, 106274 (2025).
- [63] Ozawa, M., Berthier, L., Biroli, G., Rosso, A. & Tarjus, G. Random critical point separates brittle and ductile yielding transitions in amorphous materials. *Proc. Natl. Acad. Sci.* **115**, 6656–6661 (2018).

ACKNOWLEDGMENTS

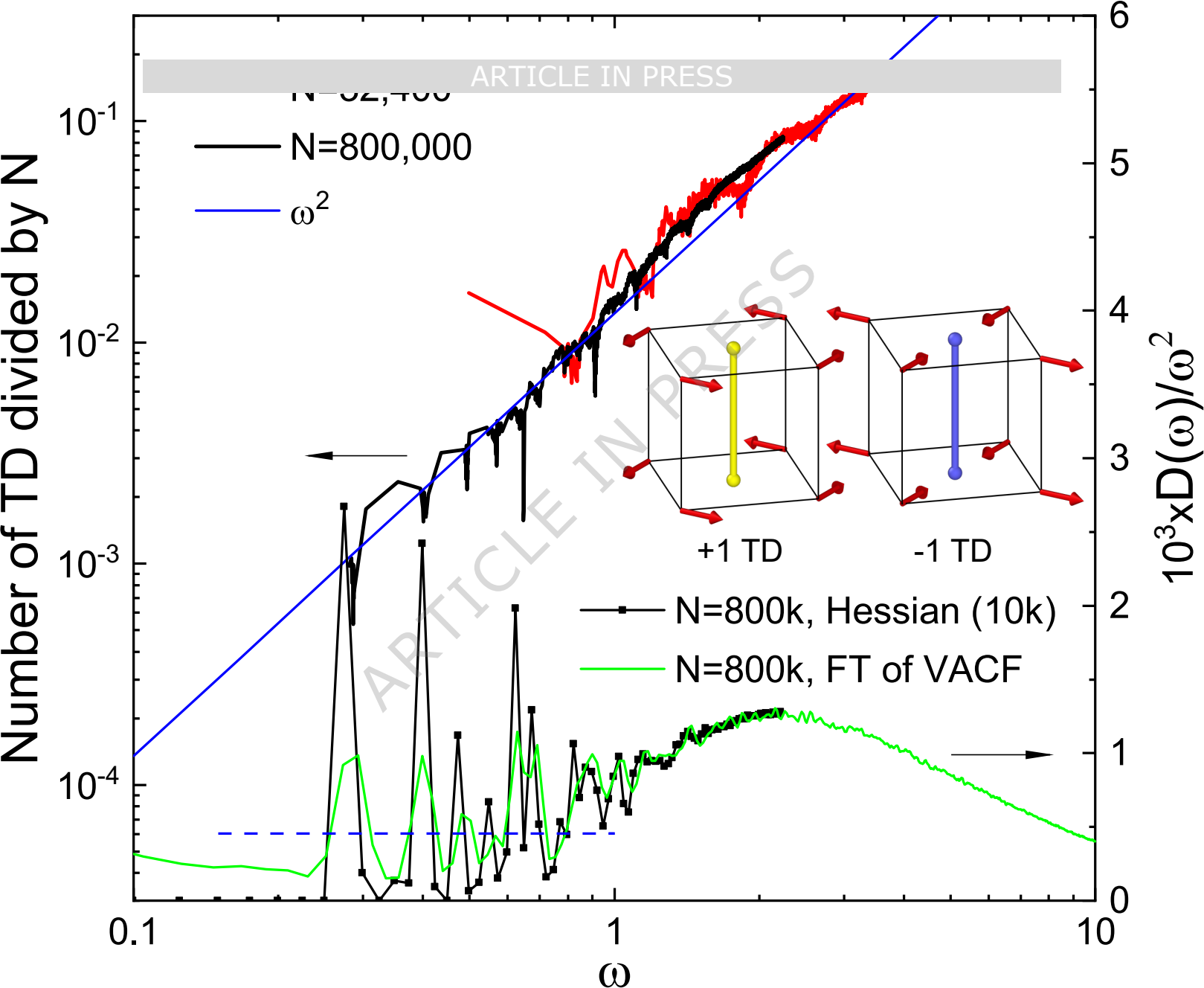
WK thanks M. Baggiooli and A. Zaccone for useful discussions and comments on the manuscript. This work was supported by the National Natural Science Foundation of China (Grant Nos. 12474184, 52031016, and 11804027). Z.W.W. thanks LIPhy-CNRS/UGA for the kind hospitality during his visit to France, and acknowledges financial support from the State Scholarship Fund of China. Z.W.W. also acknowledges support by the supercomputing center at SSS-BNU, where part of the calculations were run, for computer time. W.K. is a senior member of the Institut Universitaire de France.

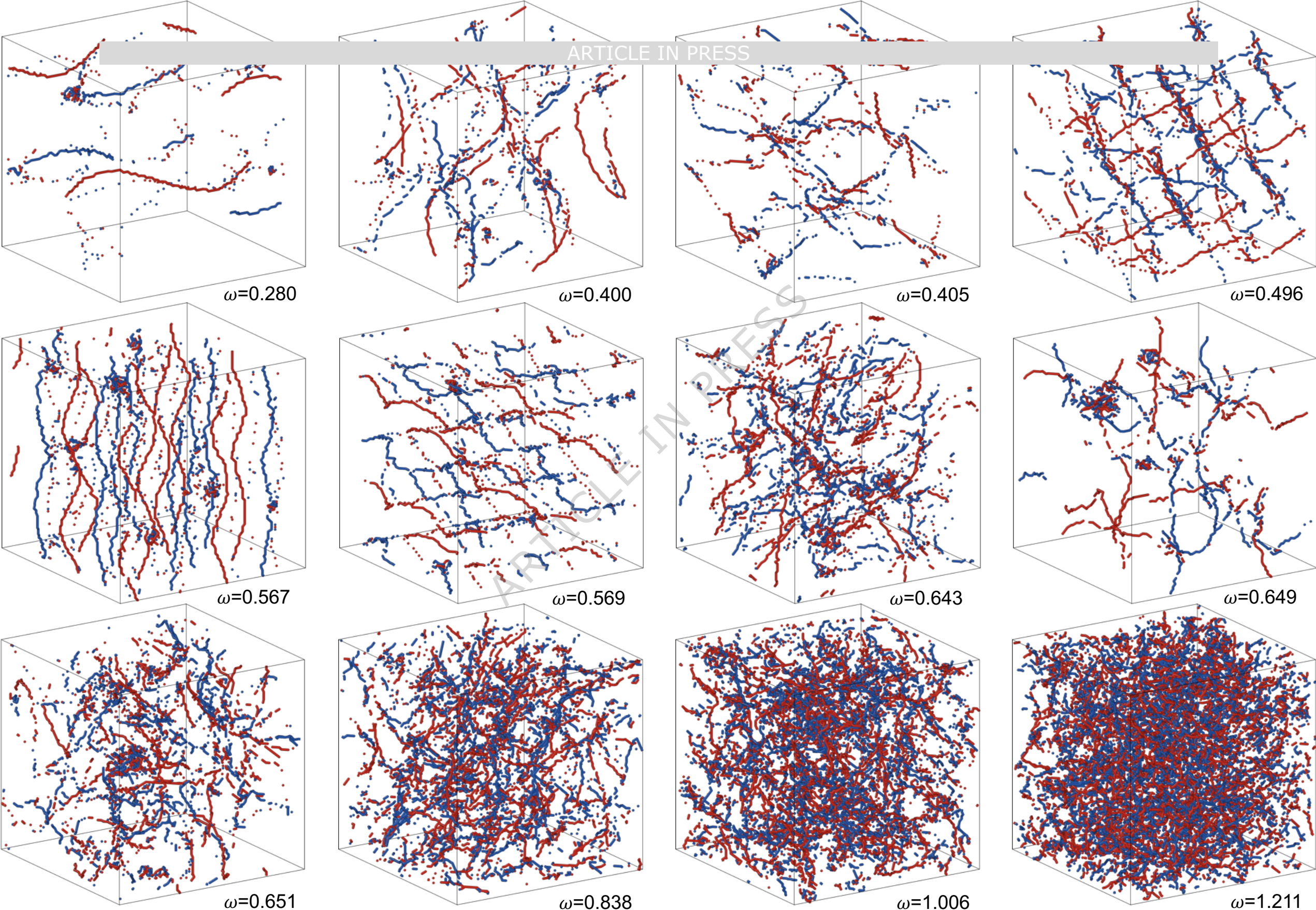
AUTHOR CONTRIBUTIONS

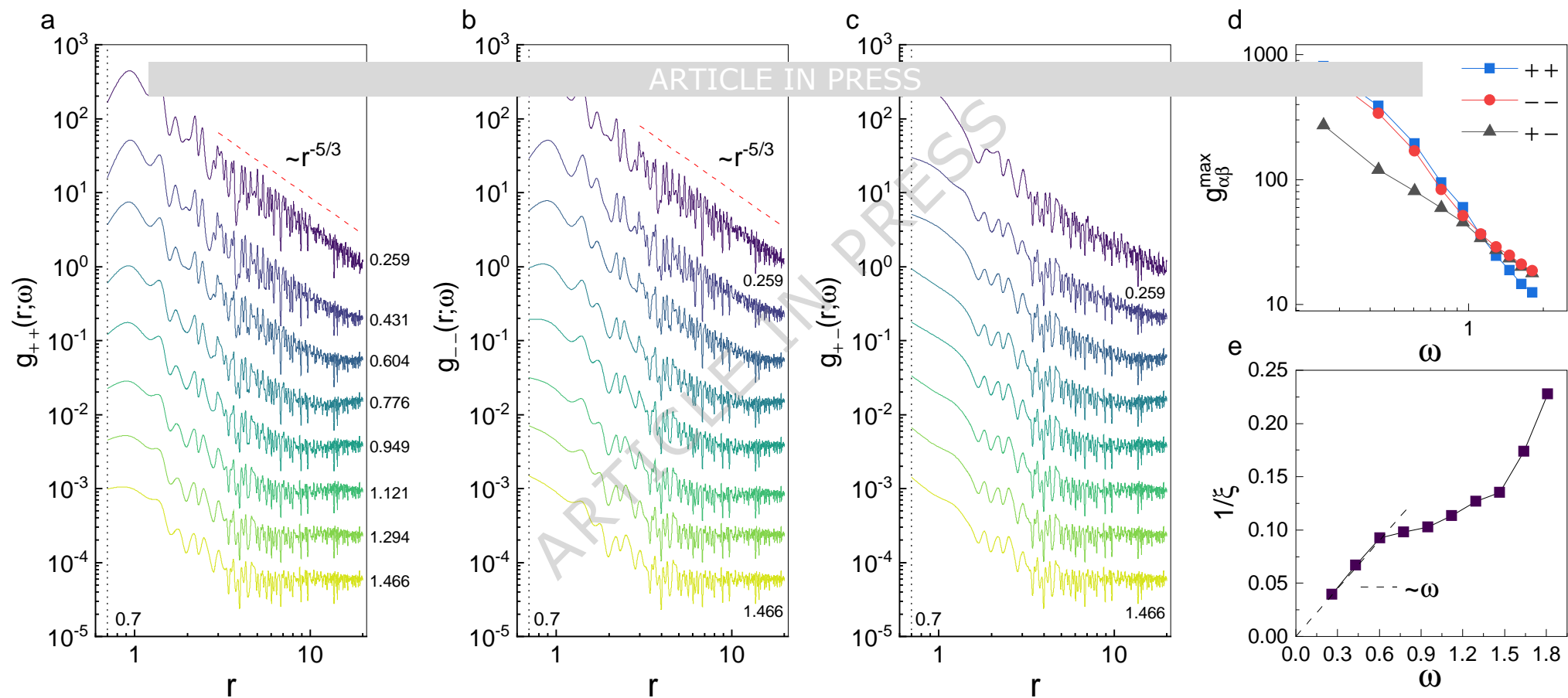
Z.W.W., J.-L.B. and W.K. designed project, performed research, analyzed data, and wrote the paper.

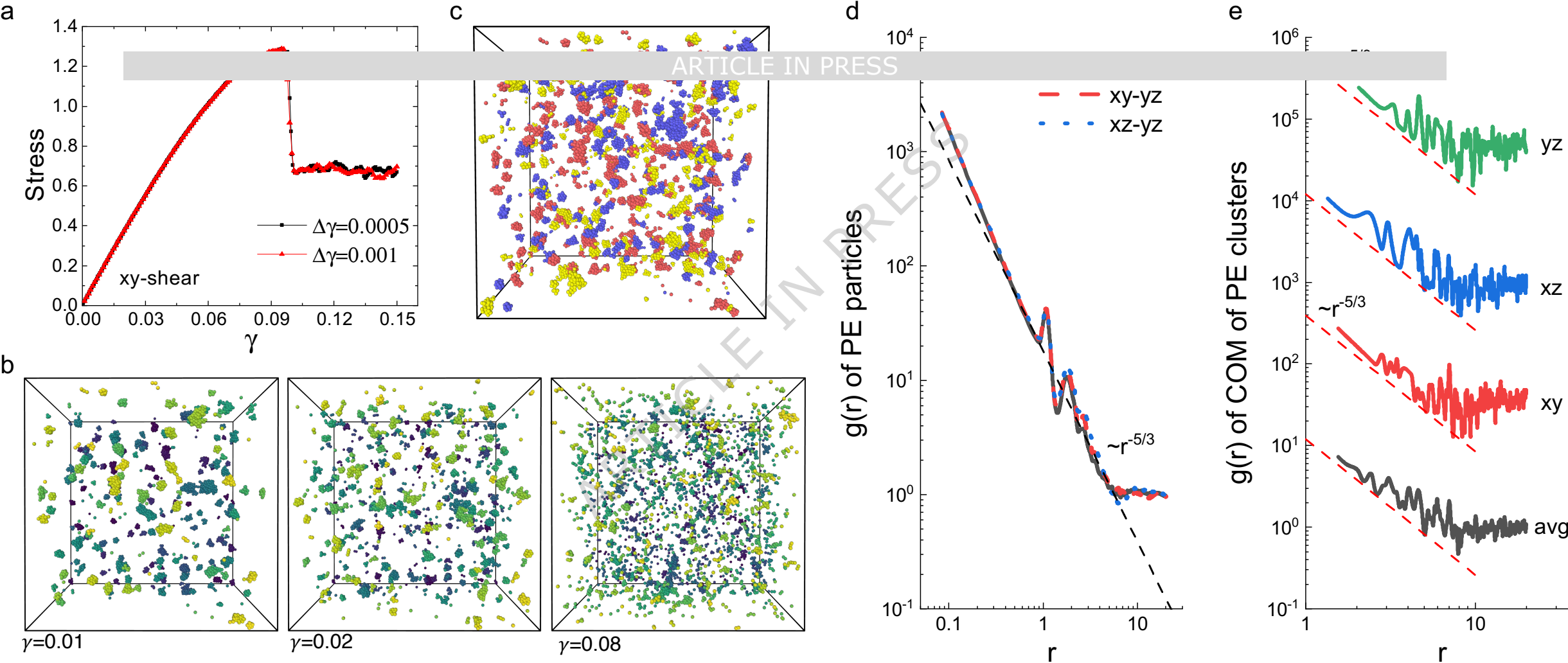
COMPETING INTERESTS

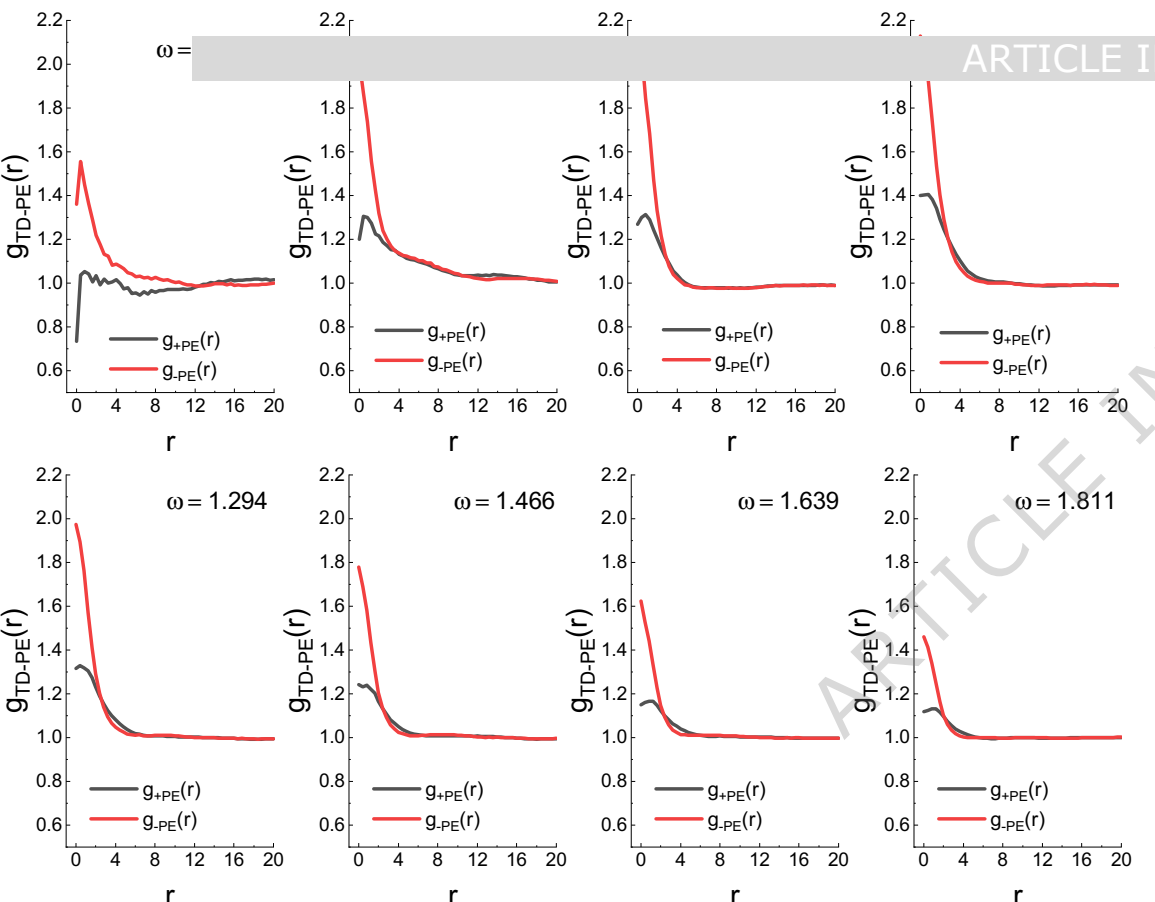
The Authors declare no Competing Financial or Non-Financial Interests.



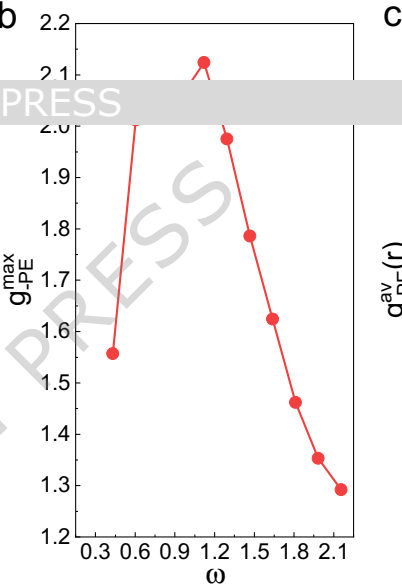
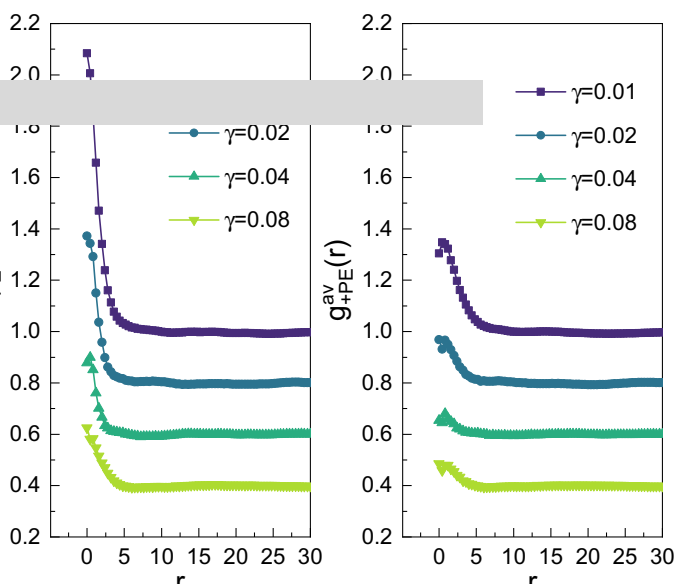
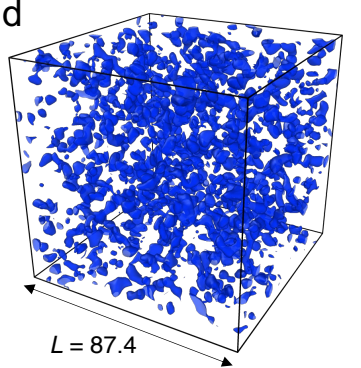






a

ARTICLE IN PRESS

b**c****d****e**